# Effects of Intermicellar Interactions on the Dissociation of Block Copolymer Micelles: SANS and NMR Studies

Gang Cheng,* Boualem Hammouda, Dvora Perahia*

The effects of intermicellar interactions on the dissociation of block copolymer micelles of polystyrene-*block*-polyisoprene in a selective solvent, decane, are investigated using small-angle neutron scattering (SANS) and ^{1}H NMR spectroscopy. This well-studied polymer is used as a model system to correlate intermicellar interactions with overall micellar stability. Decane is a preferential solvent for polyisoprene (PI) and drives the association of the polystyrene (PS) blocks, resulting in spherical micelles with a PS core and a Gaussian PI corona. The dissociation of the PS–PI micelles is triggered by increasing temperature, while the intermicellar interactions are controlled by varying the polymer concentration and modulating temperature. With increasing temperature, the cores of the micelles first swell, followed by a breakdown to smaller micelles, with similar shapes, that eventually dissociate into single molecules. Herein, it is shown for the first time that enhancing the intermicellar interaction delays the dissociation process of the micelles.
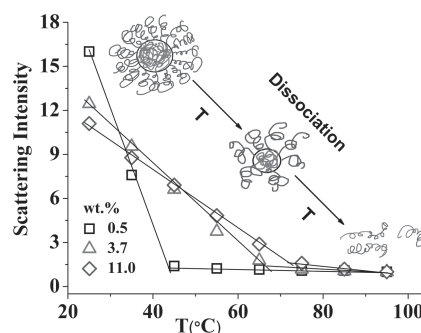
1. Introduction

Polymeric assemblies have a large number of current and potential applications, including use as templates for the synthesis of metal nanoparticles,[1] the preparation of mesoporous materials,[2] and as drug-delivery vehicles,[3,4] due in part to their structures that consist of compartments with tunable properties. Understanding the structures and dynamics of polymeric assemblies is crucial in defining their use in specific applications. For example, the core–shell architecture of block copolymer micelles enables the polymer to incorporate drugs in the core, where the corona or the part exposed to the solvent would be modified to target a specific membrane. Upon arriving at the desired site, drugs may be released through dissociation of polymer micelles triggered by various factors, such as temperature, ionic strength, and pH.[5,6] Of particular importance to their use are the factors that underlie their stability, beyond the selective interactions of the blocks with the solvent.

Over the past decade, significant work has been devoted to determining the morphology and internal structure of block copolymer micelles,[7–12] among which are a few recent studies that compared experimental results with thermodynamic models of micelle structures.[10–13] The wealth of structures that can be prepared is further enriched by metastability, particularly for micelles with a crystalline or a glassy core, where the exchange of polymer chains between micelles is very slow.[14–16] Controlling the response of block copolymer micelles requires an in-depth understanding of the association/

Dr. G. Cheng
Beijing Key Laboratory of Bioprocess and College of Life Science and Technology, Beijing University of Chemical Technology, Beijing, 100029, China
E-mail: gchengbuct@gmail.com
Dr. G. Cheng, D. Perahia
Materials Science and Engineering Program and Chemistry Department, Clemson University, SC, 29634, USA
E-mail: dperahi@clemson.edu
Dr. B. Hammouda
Center for Neutron Research, National Institute of Standards and Technology Gaithersburg, MD, 20899–6102, USA

dissociation process and precise control over the structure. Similar to low-molecular-weight surfactants, diblock copolymers in a selective solvent exhibit a critical micellar concentration (CMC) and temperature (CMT).[17] In comparison to surfactant micelles, the dynamics of block copolymer micelles at equilibrium show more complex behaviors, and are affected by additional factors, such as polydispersity and accessible conformations, due to the nature of polymer chains.[18–20] The micellization of diblock copolymers studied by computer simulation suggested that both the stepwise insertion–expulsion of single polymer chains and fusion/fission of whole micelles contributed to the redistribution of the micellar size to the equilibrium one.[21] A temperature- and pH-jump study of dual responsive diblock copolymers found that the micelle fusion/fission mechanism was responsible for micellization induced by the pH jump, and a single-chain insertion/expulsion process was observed in temperature-jump experiments.[22] Direct dissolution of poly(butadiene)-*block*-poly(ethylene oxide) in an ionic liquid resulted in large, polydisperse aggregates that relaxed upon annealing into smaller, stable spherical micelles via the fusion/fission mechanism.[18] Despite the wealth of studies, the mechanism of micelle formation and dissociation of diblock copolymer remains unresolved.[23] The distinction between the two mechanisms appears to be system specific and often both co-exist.

One exciting, unresolved aspect — the effect of intermicellar interactions on the rate and temperature of dissociation — is probed in this study. Intermicellar interactions pertain to possible cooperative behavior either between the micelles themselves or to micelles at biological interfaces. It has been shown that the intermicellar interactions play an important role in the determination of the phase behavior, rheology, and dynamics of block copolymer micelles.[24–26] A time-resolved SANS study of molecular exchange in 15 wt% polystyrene-*block*-poly(ethylene-*alt*-propylene) diblock copolymer micelles showed a slower exchange rate than in dilute solutions.[26] This is contrary to the concentration-independent, single-chain, insertion–expulsion model for block copolymer micelles, as was predicted by theory[27] and supported by other experimental work.[18–20]

In contrast to these studies, the current work uses NMR spectroscopy and SANS to follow the impact of interactions as exerted by increasing concentration of the polymer; SANS provides spatial information describing the shape and packing of the aggregates, as well as input into the conformation of the molecules in solution, and NMR spectroscopy provides dynamic information. NMR spectroscopy provides a unique insight into the dynamics not only in the micelle phase but also in the molecular solutions. Here we choose a well-characterized block copolymer micelle systems,

polystyrene-*block*-polyisoprene in decane,[28] to explore the influence of polymer concentration on the dissociation of block copolymer micelles. Previous studies of the dissociation of PS–PI diblock copolymer micelles in organic solvents have focused on either dilute solutions[9] or highly concentrated ones where the micelles were in an ordered state.[29] With increasing concentration of nonionic micelles, the intermicellar interaction increases, as long as no phase transition takes place.

The current work probes the impact of intermicellar interactions on the dissociation of PS–PI micelles. The system was followed as a function of temperature in concentrations ranging from that of an isolated micelle to interacting assemblies. PS–PI was chosen since this diblock has been well characterized and therefore allowed us to focus on the impact of the interactions. The impact of intermicellar interactions on the dissociation process was monitored by small-angle neutron scattering (SANS), monitoring the scattering intensity with increasing temperature. Using ^{1}H NMR spectroscopy we measured the change of the mobility of PS and PI chains as the dissociation progressed. Together, the results of these two techniques revealed for the first time that increasing the concentration of the polymer slowed down the process of dissociation.

2. Experimental Section

2.1. Materials

PS–PI diblock copolymers were synthesized by anionic polymerization.[25] SANS studies were carried out on an asymmetric diblock with a molecular weight of 27 800 g mol^{-1} and a polydispersity of 1.03, where the styrene block is 10 000 g mol^{-1} and the isoprene block is 17 800 g mol^{-1}. NMR spectroscopy measurements were carried out on a polymer with an overall molecular weight of 34 900 g mol^{-1} and a polydispersity of 1.03, where the styrene block is 16 500 g mol^{-1} and the isoprene block is 18 400 g mol^{-1}. Measurements are done separately on different copolymer batches to avoid any issues of degradation of the PI. Decane (D$_{22}$) (Cambridge Isotope Laboratories, Inc. MA USA) was used.

2.2. Small-Angle Neutron Scattering (SANS)

SANS measurements were performed in the Center for Neutron Research at the National Institute for Standards and Technology (NCNR) on NG3 SANS 30m with a sample-to-detector distance of 910 cm and a neutron wavelength of $\lambda = 6$ Å ($\Delta\lambda/\lambda \approx 0.15$), spanning a q range of (0.00436 to 0.0491 Å^{-1}). Using the natural contrast between PS (the scattering length density of PS is 1.40×10^{-6} Å^{-2}), PI (2.64×10^{-7} Å^{-2}), and *d*-decane (6.60×10^{-6} Å^{-2}), the total scattering function of the whole micelle, comprised of both a core and a shell, was followed as a function of temperature. All scattering data were corrected for background, empty cell scattering, and sample transmission. Solvent scattering,

Effects of Intermicellar Interactions on the Dissociation of Block Copolymer Micelles:...

Macromolecular
Chemistry and Physics

www.mcp-journal.de

normalized to its transmission and measured separately at each temperature, was then subtracted. All solutions exhibited isotropic distribution. One-dimensional patterns were obtained through radially averaging the detector area. The temperature was controlled to ±0.2 °C using a water bath and was varied from 25 to 95 °C at intervals of 10 °C. With each temperature reading, the solutions were annealed for at least 25 min prior to data collection.

2.3. SANS Analysis

Neutron analysis required the use of several form factors that have been previously derived, including that of a Gaussian chain of a polymer in dilute solution,[7] the Ornstein-Zernike description[27] of polymers in semi-dilute solutions, and the form factor for a core–shell micelles.[7] These are briefly reviewed here for convenience. The form factor of a Gaussian chain is given by:[7]

$$P(q) = \frac{e^{-x} + x - 1}{x^2} \tag{1}$$

In Equation 1, $x = (qR_g)^2$, where R_g is the radius of gyration of the polymer chain; $q = 4\pi \sin\theta / \lambda$, where 2θ is the scattering angle.

As the concentration of the polymer is increased, the scattering from a semi-dilute solution is described by an Ornstein–Zernike equation:[27]

$$I(q) = \frac{I(0)}{1 + (\zeta q)^2} \tag{2}$$

where $I(0)$ is the scattering intensity at zero angle and ζ is the correlation length.

With further increase of the concentration of the polymers, micelles are formed. For the monodisperse core–Gaussian chain model, the scattering intensity is given by:[7]

$$I(q) = nP(q)[1 + \beta(q)(S(q) - 1)] \tag{3}$$

where n is the number-density of particles, and $\beta(q) = |\langle F(q) \rangle|^2 / \langle |F(q)|^2 \rangle$, $P(q) = |\langle F(q) \rangle|^2$, where $\langle |F(q)|^2 \rangle = N_{agg}^2 [\rho_s^2 P_s(q, R) + \rho_c^2 P_{cc}(q) + 2\rho_s \rho_c P_{sc}(q)]$.

2.3.1. Form Factor of Core–Gaussian Chains Model

The scattering function of a spherical block copolymer micelle with a dense core and a corona of polymer chains obeying Gaussian statistics was described analytically, as shown by Pedersen and Gerstenberg:[7]

$$P(q) = N_{agg}^2 \beta_s^2 P_s(q, R_c) + N_{agg} \beta_c^2 P_c(q, R_g)$$
$$+ N_{agg}(N_{agg} - 1)\beta_c^2 P_{cc}(q, R_c, R_g) + 2N_{agg}^2 \beta_s \beta_c P_{sc}(q, R_c, R_g) \tag{4}$$

where N_{agg} is the aggregation number and β_s and β_c are the excess scattering length of blocks in the core and in the corona, respectively. They are calculated as $\beta_s = V_s(\rho_s - \rho_{solv})$ and $\beta_c = V_c(\rho_c - \rho_{solv})$, where $V_s = 15\,950$ Å^3 and $V_c = 32\,480$ Å^3 are the dry volume of one block in the core and corona, respectively. $\rho_s = 1.40 \times 10^{-6}$ Å^{-2}, $\rho_c = 2.64 \times 10^{-7}$ Å^{-2}, and $\rho_{solv} = 6.60 \times 10^{-6}$ Å^{-2} are the scattering length densities of core forming blocks, blocks

in the corona, and the solvent, respectively. $P_s(q, R_c)$ is the form factor of the spherical core with the radius R_c.

$$P_s(q) = \Phi(q, R_c)^2 = \left[\frac{3}{(qR_c)^3} (\sin(qR_c) - qR_c \cos(qR_c)) \right]^2 \tag{5}$$

$P_c(q, R_g)$ is the form factor of the Gaussian chain (Equation 1) in the corona with radius of gyration, R_g.

The mimicking of the non-penetration of the Gaussian chains is accomplished by starting from a distance dR_g away from the surface of the core, where d is close to unity.[7] In this study, d was set to 1.0. The interference term between core and corona chains is expressed as:

$$P_{sc}(q, R_c, R_g) = \Phi(q, R_c)\frac{1 - e^{-x}}{x}\frac{\sin[q(R_c + dR_g)]}{q(R_c + dR_g)} \tag{6}$$

The interference term between the chains in the corona $P_{cc}(q)$ is given by

$$P_{cc}(q, R_c, R_g) = \frac{(1 - e^{-x})^2}{x^2}\left[\frac{\sin[q(R_c + dR_g)]}{q(R_c + dR_g)} \right]^2 \tag{7}$$

2.3.2. Hard Sphere Structure Factor

The structure factor depends on the particle interaction potential. The Percus–Yevick[7] hard sphere interaction potential was used to approximate the interactions between micelles. In this case the structure factor is given by:

$$S(q) = \frac{1}{1 + 24\eta G(2qR_{hs}) / (2qR_{hs})} \tag{8}$$

In this equation:

$$G(x) = \frac{\alpha(\sin x - x\cos x)}{x^2}$$
$$+ \beta(2x\sin x + (2 - x^2)\cos x - 2)$$
$$+ \gamma\{-x^4\cos x + 4[(3x^2 - 6)\cos x + (x^3 - 6x)\sin x + 6]\} \tag{9}$$

where $\alpha = \frac{(1 + 2\eta)^2}{(1 - \eta)^4}$, $\beta = \frac{-6\eta\left(1 + \frac{\eta}{2}\right)^2}{(1 - \eta)^4}$, and $\gamma = \frac{\eta\alpha}{2}$.
R_{hs} is the hard sphere interaction distance, and η is the hard sphere volume fraction.

2.4. NMR Spectroscopy

NMR spectroscopy experiments were carried out on an Oxford 500 spectrometer operating at 500 MHz for protons. The temperature was controlled to ±0.5 °C. It varied from 25 to 90 °C, with a 10 °C interval. No sign of degradation of PS–PI was observed after comparing the NMR spectrum before and after the temperature experiment.

3. Results and Discussion

3.1. SANS Studies

SANS measurements of PS–PI (10k–17.8k) in decane were conducted at concentrations ranging from 0.5 to 11.0 wt%
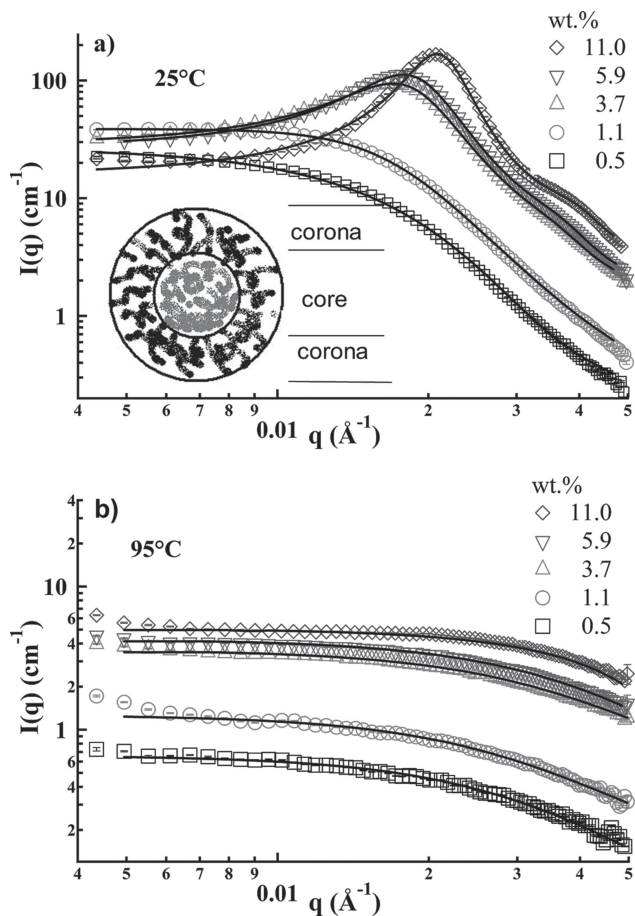
Figure 1. Representative SANS patterns at: a) 25 °C, and, b) 95 °C. The continuous lines are fits to a model of a homogenous core with many Gaussian chains attached in Figure 1a and to a Debye random coil function or an Ornstein–Zernike equation in Figure 1b.

at temperatures between 25 and 95 °C. The scattering profiles as a function of concentration at two temperatures, 25 and 95 °C, are presented in Figure 1. At 25 °C, the scattering pattern at the lower concentrations was featureless, while with increasing concentration the patterns became significantly more structured as intermicellar interactions kicked in. Within the micellar regime, an interaction peak developed and shifted to higher q values (smaller dimensions) with increasing concentration, as shown in Figure 1a. All scattering profiles at 25 °C showed similar q dependence at higher q, attributed to the scattering from the micelle/solvent interface. The Porod exponent was not extracted due to limited q range; however an exponent of −4 is expected for a sharp interface. With increasing temperature, the scattering patterns changed from that of well-defined micelles with a form factor consistent with spherical core–shell micelles, as expected for PS–PI in decane, to that of unassociated molecules. The data within the micellar phase were analyzed in terms of a homogenous

core–Gaussian chain model (Equation 4).[7] The results of the fittings are presented as solid lines in Figure 1a.

The scattering intensity at 95 °C (Figure 1b) was significantly lower than that of the corresponding solutions at 25 °C. The intensities at $q = 0$ were also proportional to the concentration of solutions. A comparison of the patterns in Figure 1a and b showed that at high temperatures the micelles dissociated into single molecules; that is, there is a critical micellar temperature (CMT) above which all the micelles dissociate. At low q, an upturn in the pattern was observed for all the solutions, except 0.5 wt% at 95 °C. This pattern upturn was interpreted in terms of the formation of instantaneous loose clusters.

Above the CMT, diblock copolymers may assume either a fully random configuration or form a "unimolecular micelle"[30] with the PS block surrounded by a PI block. A random coil form factor (Equation 1) described best the SANS patterns for 0.5 wt% at 95 °C, shown in Figure 1b as a solid line, and specified the sizes of the free polymers in solution. The Debye form factor used to describe the scattering from a single polymer chain in a theta solvent also fit the current data at high temperatures quite well, suggesting, at first approximation, that decane swelled the PS blocks at 95 °C. A polymer chain in a theta solvent assumes random-walk coil dimension. For a diblock copolymer with $\bar{M}_w$ of 27 800 g mol^{-1}, $R_g = 60$ Å (obtained from fitting of the Debye form factor to the SANS curve of 0.5 wt% solution at 95 °C), the overlap concentration is estimated as $c^* = M_w / NV = 6$ wt%, where $N = 6 \times 10^{23}$, and $V = \frac{4\pi R_g^3}{3}$. In the dilute regime, no interaction was observed, whereas in the semi-dilute regime, the onset of interaction was detected. We used the Ornstein–Zernike function (Equation 2), to model the semi-dilute regime, and the correlation length was extracted.[31] The SANS data of both the 0.5 and 1.1 wt% solutions were best described by the Debye function, (i.e., non-interacting chains), where the 3.7, 5.9, and 11.0 wt% were described by the Ornstein–Zernike model. Under the full contrast condition, as in the current study, the coherent scattering cross-section corresponds to a total scattering function, which consists of inter- and intramolecular correlations between monomers.[31] In the dilute solution regime, the intramolecular correlations (form factor) often dominate, while in the semi-dilute solutions, the Ornstein–Zernike function, which describes the intermolecular correlations, is adopted. The results from the fitting are plotted in Figure 2a. The correlation length decreased with increasing concentration and, due to limited data points, a scaling relation was not extracted. Statistical error bars correspond to one standard deviation.

Figure 2b shows the concentration dependence of both the micellar core size and the R_g of polymers in the shell at 25 °C. In the temperature and concentration range where the form factor of an isolated micelle dominated the
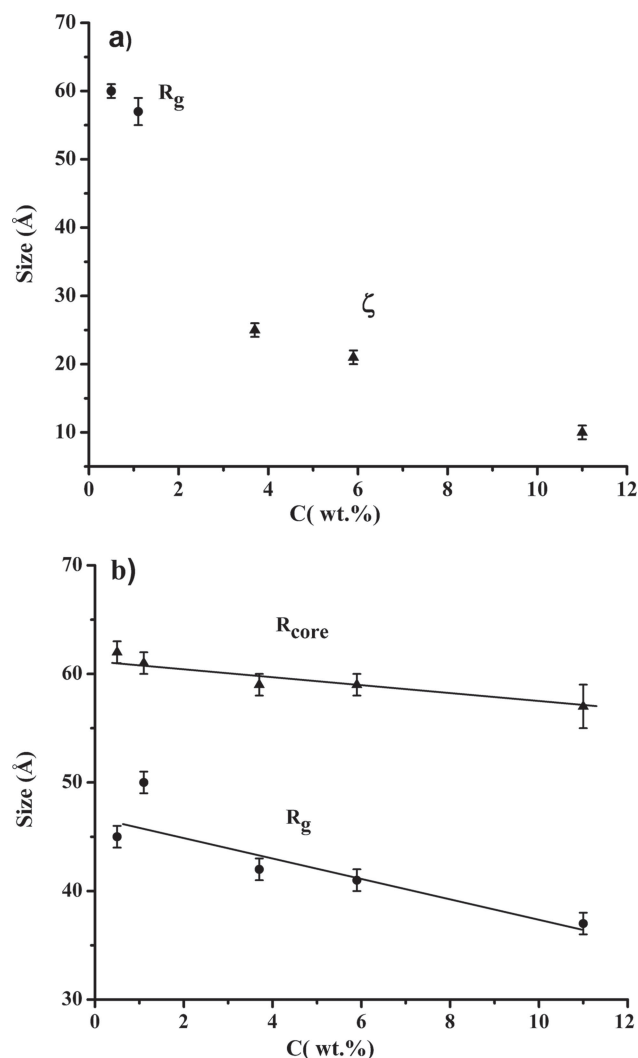
Effects of Intermellar Interactions on the Dissociation of Block Copolymer Micelles:...

Macromolecular
Chemistry and Physics

www.mcp-journal.de

Figure 2. a) Concentration dependence of the core radius and the R_g of the PI in the shell at 25 °C. b) R_g of block copolymers in dilute solutions and the correlation length ξ in semi-dilute solutions at 95 °C.
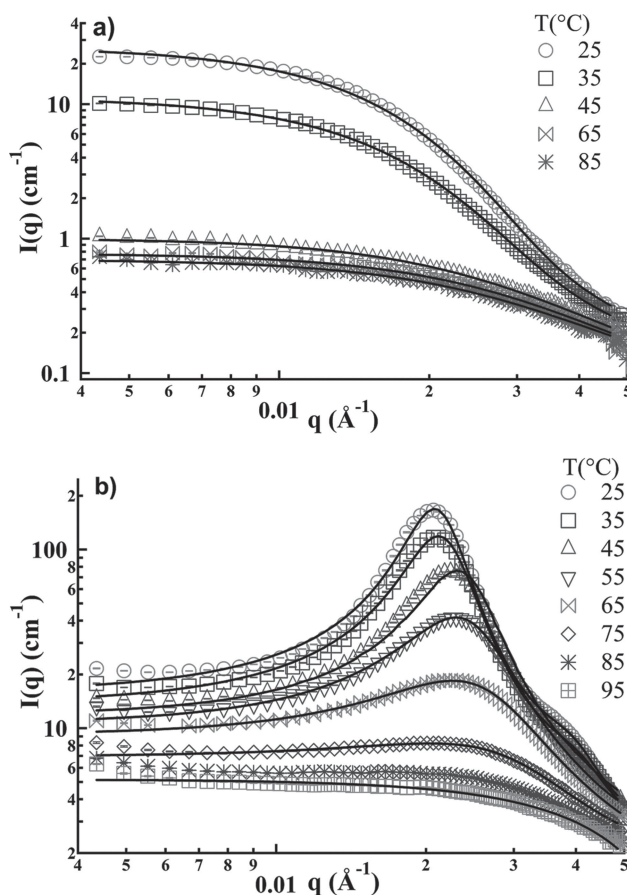

Figure 3. Representative SANS data of: a) 0.5 wt%, and, b) 11.0 wt% solutions at different temperatures. The continuous lines are fits to a model of a homogenous core with many Gaussian chains attached.

scattering patterns, the micellar core radius (R_c) and the radius of gyration of the polymers (R_g) in the shell were extracted. A hard sphere interaction term (Equation 8) was added at higher concentrations (3.7, 5.0, and 11.0 wt%), where the intermicellar interaction became apparent.[7] The polymers in the corona were similar to those in a semi-dilute solution where their radius of gyration decreases with increasing concentration due to screening of excluded volume interactions.[32] The increase in concentration results in increased intermicellar interactions. The unperturbed radius of gyration of the PI blocks was calculated as $R_g = \sqrt{Nb^2/6} = 42$ Å and the mean square end-to-end distance of the PS blocks was calculated as $R = \sqrt{Nb^2} = 67$ Å, where N is the number of Kuhn segments b, and $b = 8.2$ Å for PI and 18 Å for PS.[33] Thus, the

PI blocks were in a stretched conformation in the corona of the micelles in dilute solutions, and with increasing solution concentration to about 4 wt%, they relaxed to the unperturbed state. However, the PI blocks continued to decrease in size with further increase of solution concentration; therefore, the repulsive interactions between PI blocks of different micelles are possibly the additional factor for the reduction of their dimensions.

The scattering profiles as a function of temperature for two concentrations, the lowest and the highest, 0.5 and 11.0 wt%, are presented in Figure 3a and b, respectively. For the data of other concentrations, see Figure S1 in the Supporting Information. For all concentrations, the scattering intensity decreased with increasing temperature, as expected when dissociation of micelles took place. As the dissociation took place, the variations of the internal structures of micelles were followed as a function of temperature for all the studied concentrations. Shown in Figure 4a and b are R_c and R_g extracted from the fitting. As a general trend, both R_c and R_g decreased with increasing

Materials
Views
www.MaterialsViews.com

Macromol. Chem. Phys. 2014, 215, 341–350
© 2014 WILEY-VCH Verlag GmbH & Co. KGaA, Weinheim
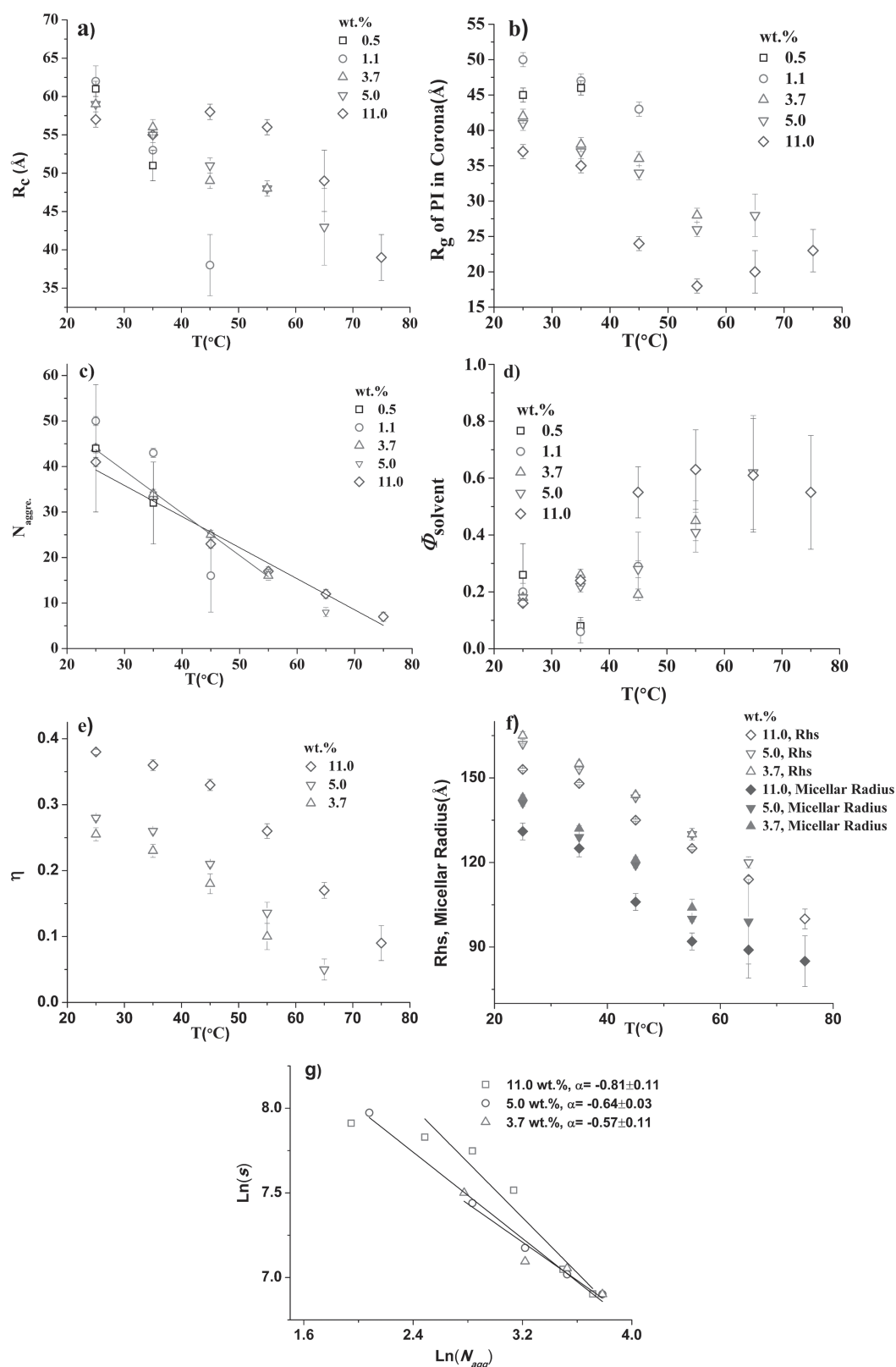
Macromolecular
Journals

345

Figure 4. Temperature dependence of: a) micellar core radius, b) R_g of the PI in the shell, c) the micelle aggregation number, d) the volume fraction of decane in the core, e) the hard sphere volume fraction, f) the hard sphere interaction distance, g) the core–shell interfacial area per chain. The straight lines in Figure 4c are fits to a linear function.

Effects of Intermicellar Interactions on the Dissociation of Block Copolymer Micelles:...

Macromolecular
Chemistry and Physics

www.mcp-journal.de

temperature. With increasing temperature, the core–shell interfacial tension decreased with a corresponding increase in solvent quality for each of the blocks, resulting in a relaxation of the polymers in the core and in the shell toward their unperturbed conformations. However, the polymers in the micelles assumed sizes which are smaller than their unperturbed conformations at higher concentrations. The decrease in dimensions of the micelles with increasing temperature is likely a conjunction of decrease in aggregation number coupled with concentration-dependent internal conformational changes.

Figure 4c displays the temperature dependence of aggregation number, as extracted from the fitting. For all concentrations, the aggregation number decreased with increasing temperature. Surprisingly, the aggregation number of micelles in concentrated solutions decreased slower with increasing temperature than that in lower concentrated solutions. To better illustrate this observation, a linear function was fitted to the temperature dependence of the aggregation number. Two representative solutions, 3.7 and 11.0 wt%, were chosen to emphasize the difference in the change of the aggregation number with temperature. As can be seen in Figure 4c, the different slopes of the straight lines suggest that intermicellar interactions affected the dissociation of the micelles. At lower concentrations, the temperature range of the micellar phase was limited and only limited data points were available.

Another consequence of raising temperature was more decane penetration into the PS core. The volume faction of decane in the PS core, $\Phi_{solvent}$, was calculated using fitted values of the aggregation number and R_c via: $1 - N_{agg}V_{PS}/(4\pi R_c^3/3)$, where N_{agg} is the aggregation number, V_{PS} is the dry volume of one PS block, and R_c is the core radius. The values of the $\Phi_{solvent}$ at temperatures below the CMTs are given in Figure 4d. The fraction of solvents in the core increased with decreasing concentrations, which was reported before[34] and was consistent with the finding that CMT was lower for lower concentration solutions. With increasing temperature, more solvents penetrated into the cores. At temperatures near the CMT, the cores became less defined, which explains the large error bars associated with the volume fraction of the solvent in the cores.

For analyzing the SANS data of 3.7, 5.0, and 11.0 wt% solutions, the hard sphere structure factor was included. The obtained volume fraction of the micelles (η) and interaction distance (R_{hs}), plotted as a function of temperature, are presented in Figure 4e and 4f, respectively. The volume fraction was proportional to the polymer concentrations and the interaction distance was inversely proportional to them. It was noted that the R_{hs} of micelles in 5.0% and 3.7% solutions became closer with the progress of dissociation of micelles. Both the volume fraction and the

interaction distance decreased with increasing temperature, consistent with dissociation of micelles. The micellar radii, calculated as $R_c + 2R_g$, of 3.7, 5.0, and 11.0 wt% solutions are also included in Figure 4f as solid symbols. The micellar radii were lower than their corresponding R_{hs}, suggesting no overlapping of micellar shells.[35]

The core–shell interfacial area per chain, calculated as $s = 4\pi R_c^2/N_{agg}$,[36] was plotted as a function of temperature for 3.7, 5.0, and 11.0 wt% solutions in Figure 4g. In lower concentrations, the temperature range of the micellar phase was limited and no meaningful information can be extracted. Assuming no solvent penetration in the core of the micelles, the aggregation number N_{agg} scales linearly with the third power of the core radius R_c.[37] Therefore, $s \sim N_{agg}^{-1/3}$. As shown in Figure 4g, the surface-area-per-chain scaled with the aggregation number as $s \sim N_{agg}^{-0.57}$, $s \sim N_{agg}^{-0.64}$, and $s \sim N_{agg}^{-0.81}$ for 3.7, 5.0, and 11.0 wt% solutions, respectively. The more negative exponent than $-1/3$ was likely caused by the penetration of decane molecules into the core of the micelles. The surface area per chain became larger as dissociation took place, which facilitated the relaxation of the polymers confined to the core–shell interface, and this was also consistent with a decreased core–shell interfacial tension as temperature increased.

To further quantitatively characterize the dissociation process and to determine the CMT of the micellar solutions, the integrated scattering intensity ($I_{int,T}$) at each temperature was normalized to the integrated intensity at 95 °C ($I_{int,95°C}$), where the solutions consisted of isolated molecules. For different concentrations, $I_{int,T}/I_{int,95°C}$ was plotted as a function of temperature, as shown in Figure 5. The normalized intensity represented an increase in scattering due to the formation of micelles. Two regions were distinguished as a function of decreasing temperature for all measured concentrations: a high temperature range characterized by a slight increase in integrated intensity, and a low temperature range characterized by a significant increase in integrated intensity. The temperature of the intercept of the two straight lines representing these two regions provided the CMT as a function of concentration, shown as an insert. The CMT increased with the increase of concentration, similar to low molar mass surfactants. The standard enthalpy of micellization was determined from the following relationship:[17]

$$\Delta H = R \frac{d\ln C}{d(1/CMT)}$$

(10)

ΔH, extracted from the plot of $\ln C$ as a function of the reciprocal of CMT (see Figure S2 in the supporting Information), is -93.7 kJ mol^{-1}. The negative enthalpy showed micelle formation to be an enthalpy-driven spontaneous process, as expected for a diblock copolymer in a selective solvent.
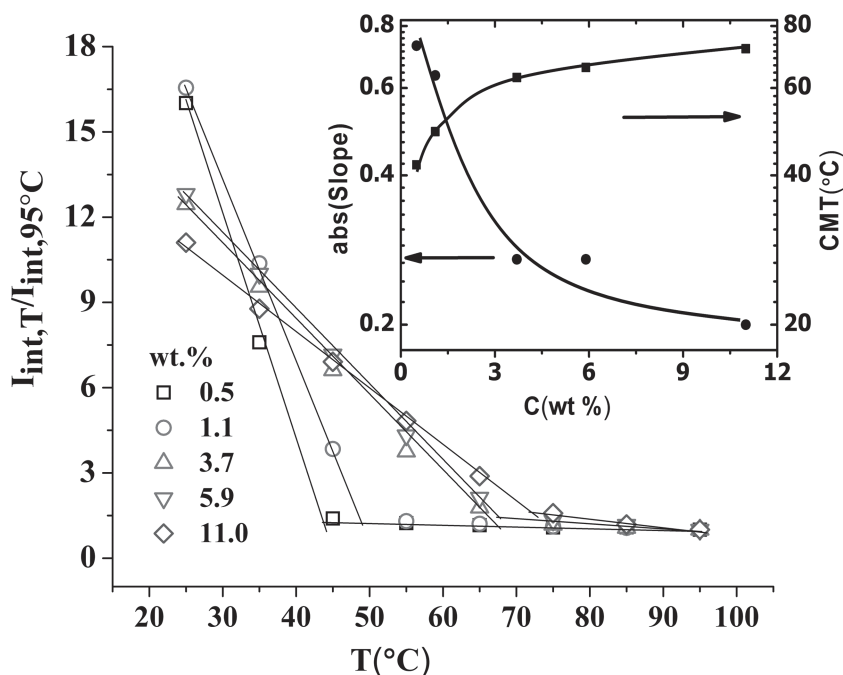
Materials
Views

www.MaterialsViews.com

Macromol. Chem. Phys. **2014**, *215*, 341–350
© 2014 WILEY-VCH Verlag GmbH & Co. KGaA, Weinheim

Macromolecular
Journals

347

Figure 5. Plot of the normalized integrated scattering intensity as a function of temperature. The inset is a plot of the slope obtained from fitting the intensity decay above CMT as a function of concentration (left axis); the concentration dependence of CMT is shown on the right axis.

The slope of the scattering intensity below the CMT (insert in Figure 5) as a function of temperature was inversely proportional to the stability range of the micelles, whereas a larger slope indicated a faster dissociation of the micelles. A comparison between the slope and the development of the interaction peak in the pattern showed that the intermicellar interaction stabilized the micelles. This was consistent with the temperature dependence of aggregation number for different concentrations. When the temperature was increased, the equilibrium between free polymers and micelles was disrupted. In the course of relaxing to a new equilibrium state, previous studies suggested that the micelles changed their aggregation numbers and sizes via two possible mechanisms: stepwise insertion/expulsion of single polymer chains and micelle fusion/fission.[23] The model of polymer insertion/expulsion yielded a single exponential decay function with a concentration-independent relaxation rate.[20,27] Other studies showed that the concentration-dependent micelle fusion/fission also contributed to the chain exchange process.[15,22] In that model, the corresponding relaxation time decreased with increasing polymer concentration, as the probability of aggregate collision increased.

Our results suggest that the intermicellar interaction slows down the dissociation process, which precludes the micelle fusion/fission mechanism under which higher concentration leads to higher relaxation rates of the polymer chains. This leaves us with the choice of the stepwise insertion/expulsion process. However, this process is known to be concentration-independent.[26] Our observation is consistent with a recent experimental study where a slower chain exchange rate between strongly interacting micelles was reported.[26] Progress has been made in understanding the origin of the slowdown[38] that considered coronal screening and the resulting increase in the osmotic pressure encountered by the expelled polymer; however, more work is still needed.[20]
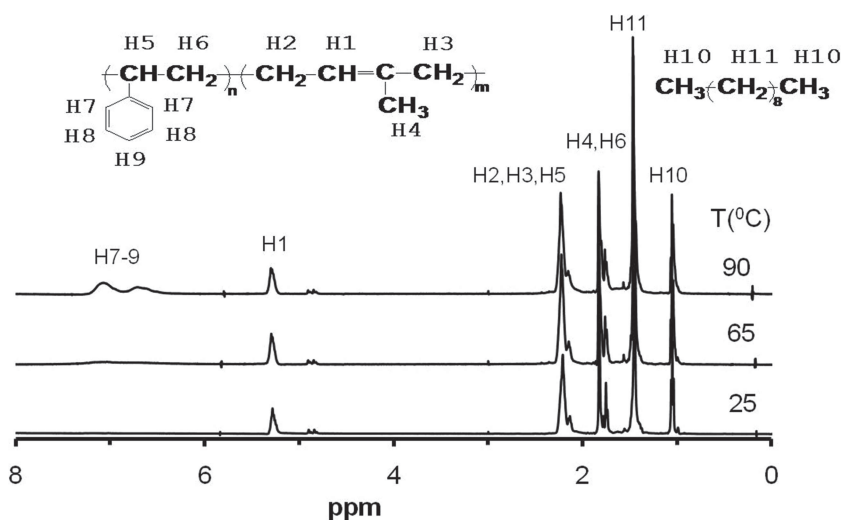
3.2. NMR Spectroscopy

As chains in the micellar core have lower mobility compared to free chains, ^{1}H NMR spectroscopy relaxation time measurements can follow the association/dissociation process.[39] The ^{1}H NMR spectrum of a 10.0 wt% solution of PS–PI in decane (a mixture of 96.0 wt% deuterated decane and 4.0 wt% protonated decane) at different temperatures is shown in Figure 6. The protonated decane was used as a probe to follow the interactions between the micelle and the solvent. The NMR spectroscopy
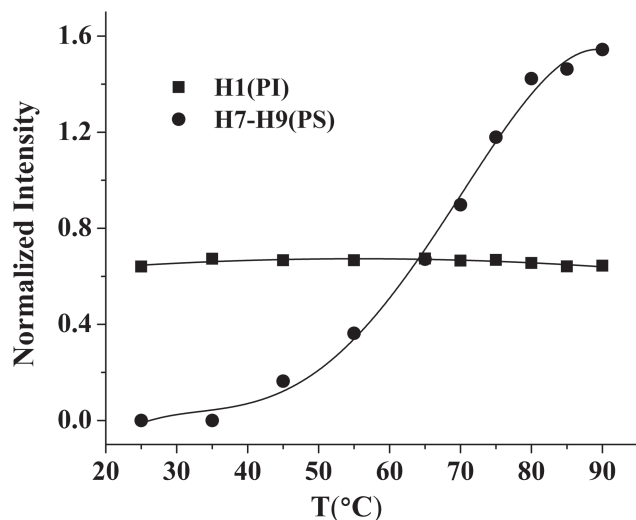

Figure 6. ^{1}H NMR spectrum of 10 wt% PS–PI in decane at different temperatures.

Effects of Intermicellar Interactions on the Dissociation of Block Copolymer Micelles:...

Macromolecular
Chemistry and Physics

www.mcp-journal.de

Figure 7. Plot of the normalized ^1H NMR spectroscopy intensity of selective protons on PS and PI as a function of temperature.

relaxation times were inversely proportional to the interaction of the chains; i.e., the magnetic relaxation of the free chains was longer than that of interacting confined chains. At 25 °C, the PS chains were confined to the core, whereas the PI blocks were dissolved in decane. Under the conditions in which the experiments were carried out, only signals that corresponded to the protons on the PI were detected. The absence of the PS signals showed that the motion of the PS block in the core was restricted and the polymer chains were in a glassy state, resulting in fast spin relaxation times that could not be detected using the conditions appropriate for liquids.

Under the same conditions, the PI was immersed in the solvent and was more fluid-like, resulting in clear signals. As shown in Figure 7, where the intensity was normalized to that of H10 of decane, the intensities corresponding to the aromatic protons on the PS assumed a different pattern than the temperature dependence of the decane signal and the PI signal. As the temperature increased, the signals of the aromatic protons on the PS gradually appeared in the spectrum due to increasing PS mobility in the core. Above 45 °C, the intensity of the signals that corresponded to the aromatic protons of the PS increased. With increasing temperature, the mobility and the solubility of the PS increased, resulting in enhanced solvent penetration into the core. This observation is consistent with the results of SANS, which has detected increases in the concentration of decane in the core. Above 80 °C, the change in intensity leveled off and approached an equilibrium value as a transition from micelles to single block copolymer chains took place. The proton signals from PI and from decane behaved similarly (Figure 7), confirming the high mobility of the PI blocks and the fast exchange of

the decane molecules between the corona and the environment. NMR studies showed that the degree of penetration of solvent into the core affected the rate of dissociation of the micelles. A CMT of 70 °C was extracted by taking the peak value on the data of the first derivative of the NMR spectroscopy intensity of PS in Figure 7. The plot of the first derivative as a function of temperature is included as Figure S3 in the Supporting Information.

4. Conclusion

Our studies of the assembling process of PS–PI in decane into micelles using SANS and NMR spectroscopy have shown that increasing concentration stabilizes the micelles via enhancing intramicellar interactions. Similar to small surfactants and diblock copolymers in other solvents, a critical micelle temperature was observed. The CMT increases with increasing concentration. The dissociation of the micelles with temperature was initiated by increased mobility of the chains in the core, followed by solvent uptake and eventually resulting in a full dissociation of the micelles. In contrast to small molecules, the dissociation of micelles is rather gradual and even in molecular solutions; the more soluble block is more dynamic in comparison with to the block with lower solubility. Overall, the study has shown that the interaction between micelles, which increases with increasing concentration of the polymer in decane, further stabilizes the aggregates, and it has suggested a model for dissociation of block-copolymer micelles via stepwise insertion/expulsion.

Supporting Information

Supporting Information is available from the Wiley Online Library or from the author.

Materials
Views
www.MaterialsViews.com

Macromol. Chem. Phys. **2014**, 215, 341–350
© 2014 WILEY-VCH Verlag GmbH & Co. KGaA, Weinheim

Macromolecular
Journals

349

[1] P. Khullar, A. Mahal, V. Singh, T. S. Banipal, G. Kaur, M. S. Bakshi, *Langmuir* **2010**, *26*, 11363.

[2] S. Manet, A. Lecchi, M. Imperor-Clerc, V. Zholobenko, D. Durand, C. L. P. Oliveira, J. S. Pedersen, I. Grillo, F. Meneau, C. Rochas, *J. Phys. Chem. B* **2011**, *115*, 11318.

[3] S. Alexander, W. M. de Vos, T. C. Castle, T. Cosgrove, S. W. Prescott, *Langmuir* **2012**, *28*, 6539.

[4] L. Y. Lin, N. S. Lee, J. H. Zhu, A. M. Nystrom, D. J. Pochan, R. B. Dorshow, K. L. Wooley, *J. Controlled Release* **2011**, *152*, 37.

[5] C. Oerlemans, W. Bult, M. Bos, G. Storm, J. F. W. Nijsen, W. E. Hennink, *Pharm. Res.* **2010**, *27*, 2569.

[6] M. Valero, C. C. A. Dreiss, *Langmuir* **2010**, *26*, 10561.

[7] J. S. Pedersen, M. C. Gerstenberg, *Colloids Surf. A* **2003**, *213*, 175.

[8] J. Bang, S. Jain, Z. Li, T. P. Lodge, J. S. Pedersen, E. Kesselman, Y. Talmon, *Macromolecules* **2006**, *39*, 1199.

[9] J. Bang, K. Viswanathan, T. P. Lodge, M. J. Park, K. Char, *J. Chem. Phys.* **2004**, *121*, 11489.

[10] I. LaRue, M. Adam, E. B. Zhulina, M. Rubinstein, M. Pitsikalis, N. Hadjichristidis, D. A. Ivanov, R. I. Gearba, D. V. Anokhin, S. S. Sheiko, *Macromolecules* **2008**, *41*, 6555.

[11] R. Lund, V. Pipich, L. Willner, A. Radulescu, J. Colmenero, D. Richter, *Soft Matter* **2011**, *7*, 1491.

[12] G. V. Jensen, Q. Shi, G. R. Deen, K. Almdal, J. S. Pedersen, *Macromolecules* **2011**, *45*, 430.

[13] E. B. Zhulina, M. Adam, I. LaRue, S. S. Sheiko, M. Rubinstein, *Macromolecules* **2005**, *38*, 5330.

[14] J. B. Gilroy, P. A. Rupar, G. R. Whittell, L. Chabanne, N. J. Terrill, M. A. Winnik, I. Manners, R. M. Richardson, *J. Am. Chem. Soc.* **2011**, *133*, 17056.

[15] L. Meli, J. M. Santiago, T. P. Lodge, *Macromolecules* **2010**, *43*, 2018.

[16] J. Schmelz, M. Karg, T. Hellweg, H. Schmalz, *ACS Nano* **2011**, *5*, 9523.

[17] P. Alexandridis, J. F. Holzwarth, T. A. Hatton, *Macromolecules* **1994**, *27*, 2414.

[18] R. Lund, L. Willner, D. Richter, E. E. Dormidontova, *Macromolecules* **2006**, *39*, 4566.

[19] J. Lu, S. Choi, F. S. Bates, T. P. Lodge, *ACS Macro Lett.* **2012**, *1*, 982.

[20] T. Zinn, L. Willner, R. Lund, V. Pipich, D. Richter, *Soft Matter* **2012**, *8*, 623.

[21] E. E. Dormidontova, *Macromolecules* **1999**, *32*, 7630.

[22] Y. F. Zhang, T. Wu, S. Y. Liu, *Macromol. Chem. Phys.* **2007**, *208*, 2492.

[23] A. G. Denkova, E. Mendes, M. O. Coppens, *Soft Matter* **2010**, *6*, 2351.

[24] A. Cambon, S. Barbosa, A. Rey-Rico, E. B. Figueroa-Ochoa, J. F. A. Soltero, S. G. Yeates, C. Alvarez-Lorenzo, A. Concheiro, P. Taboada, V. Mosquera, *J. Colloid Interface Sci.* **2012**, *387*, 275.

[25] E. van Ruymbeke, A. Pamvouxoglou, D. Vlassopoulos, G. Petekidis, G. Mountrichas, S. Pispas, *Soft Matter* **2010**, *6*, 881.

[26] S.-H. Choi, F. S. Bates, T. P. Lodge, *Macromolecules* **2011**, *44*, 3594.

[27] A. Halperin, S. Alexander, *Macromolecules* **1989**, *22*, 2403.

[28] C. Lai, W. B. Russel, R. A. Register, *Macromolecules* **2001**, *35*, 841.

[29] M. J. Park, K. Char, J. Bang, T. P. Lodge, *Macromolecules* **2005**, *38*, 2449.

[30] T. P. Lodge, *Macromol. Chem. Phys.* **2003**, *204*, 265.

[31] G. D. Wignall, Y. B. Melnichenko, *Rep. Prog. Phys.* **2005**, *68*, 1761.

[32] G. Cheng, W. W. Graessley, Y. B. Melnichenko, *Phys. Rev. Lett.* **2009**, *102*.

[33] M. Rubinstein, R. H. Colby, *Polymer Physics*, Oxford University Press, Oxford/New York **2003**.

[34] Y. Liu, S.-H. Chen, J. S. Huang, *Macromolecules* **1998**, *31*, 2236.

[35] A. V. Korobko, W. Jesse, S. U. Egelhaaf, A. Lapp, J. R. C. van der Maarel, *Phys. Rev. Lett.* **2004**, *93*, 177801.

[36] Z. L. Li, E. E. Dormidontova, *Soft Matter* **2011**, *7*, 4179.

[37] N. Dan, M. Tirrell, *Macromolecules* **1993**, *26*, 4310.

[38] A. Halperin, *Macromolecules* **2011**, *44*, 5072.

[39] M. Vamvakaki, D. Palioura, A. Spyros, S. P. Armes, S. H. Anastasiadis, *Macromolecules* **2006**, *39*, 5106.

www.MaterialsViews.com